Indian Journal of Fibre & Textile Research
Vol. 44, March 2019, pp. 45-50

Physicochemical characterization of natural hydroxyapatite/ cellulose composite

Majed M Alghamdi[1], Nasser S Awwad[1], Abdullah A Al-Karim Al-Shara'ey[2], Hisham S M Abd-Rabboh[1] & Sherif M A S Keshk[1, 3, a]

[1] Chemistry Department, Faculty of Science, King Khalid University, P.O. Box 9004, Abha 61413, Saudi Arabia

[2] Chemistry Department, Faculty of applied Science, Taiz University, Taiz, Yemen

[3] Basic Science Department, Institute of Environmental Studies and Research, Ain-Shams University, Abbassia, Cairo 11566, Egypt

Received 21 April 2017; revised received and accepted 1 November 2017

The natural hydroxyapatite (HAp, activated at different temperatures)/ cellulose composites have been prepared by using sonication method to improve the physical properties of the cellulose fibre. The molecular level interaction and the physical properties of the hydroxyapatite/cellulose composite are examined using FTIR, X-ray diffraction, SEM, and thermal analysis. The absorption bands at around 660 cm^{-1} confirm the O–P–O bending vibration in the HAp/cellulose composites. There is a difference in the *d*-spacing of the HAp /cellulose composite, indicating that the HAp is reactive towards cellulose. SEM indicates that HAp could penetrate the cellulose network structure to form particles that is helpful to improve the mechanical properties of the cellulose. The porosities of HAp/cellulose composites decrease, and their compressive strength increase as compared to those of cellulose. Thermogravimetric analysis confirms the highest thermal stability of the prepared composites.

Keywords: Cellulose, Composite, Hydroxyl appatite, Sonication method, Thermal analysis, X-ray diffraction

1 Introduction

With an increasing demand for cellulose in the industrial market and simultaneous pressure to address the issue of its sustainability, most of the composite substances prepared from organic and inorganic phases have attracted much attention[1–3]. A starch/cellulose composite showed higher transition temperature and crosslink density than those of cellulose [3]. The presence of metal oxides such as ZnO, NiO, and TiO_2 in cellulosic fibres modifies the physical properties of cellulose [2-4]. On the other hand, hydroxyapatite (HAp) is considered as an inorganic component of the natural bone and is mostly being used in the field of tissue engineering because of its excellent biocompatibility, bioactivity, non-inflammatory properties and nontoxicity[5,6]. Hydroxyapatite is a hydroxyl end member of the apatite group with the formula $Ca_{10}(PO_4)_6(OH)_2$. HAp contains the main mineral component of human bones and teeth in which mature bone consists of 60–70% of HAp[7]. HAp is one of the most attractive materials for human hard tissue implants[8]. The synthetic hydroxyapatite is widely used as a coating material on the surface of implant metals/alloys to connect the implant material and bone to promote osteointegration[9]. Besides its biocompatibility, HAp is of much interest as a drug-delivery medium[8]. For example, synthetic porous hydroxyapatite implants are used for the local drug delivery in bones [10]. Nanosized composite rods with a length of 300 nm and a width of 20 nm have been produced by the deposition of 22–77 wt% of synthetic hydroxyapatite on cellulose nanocrystals[11]. The produced composites exhibited improved mechanical strength compared to those of crustacean exoskeletons and the potential for bone regeneration. Synthetic HAp has been known to have difficulty in practical use as it exists in the form of the white powder and it shows irregular dispersion in cellulose[12]. The chemical composition of synthetic hydroxyapatite is 1.4 wt% for both CaO and P_2O_5, that is lower than those in natural hydroxyapatite[13–16]. The concentrations of CaO and P_2O_5 are around 54.5 wt% and 41.6wt% respectively in natural hydroxyapatite. However, studies on the combination of the natural HAp with cellulose have not been conducted so far. In this work, the natural HAp derived from camel bones is blended with the cellulosic fibre for the first time. The physicochemical characterization of the HAp/cellulose composite is performed using Fourier transform infrared (FTIR), X-

[a]Corresponding author.
E-mail: keshksherif@gmail.com

ray diffraction (XRD), scanning electron microscopy (SEM), and thermogravimetric analysis (TGA).

2 Materials and Methods

2.1 Materials

Cotton linters (DP 950) were purchased from Sigma-Aldrich. All AR grade chemicals were purchased from Sigma-Aldrich© and used without any further purification/ treatment.

2.2 Activation of Natural Hydroxyapatite

The camel bones samples were cut into small pieces and immersed in dilute acetic acid for 24 h for the efficient removal of fat and tissues from bones. They were then washed with distilled water and dried at 220°C for 48 h, and finally were cooled, grounded, and sieved through a membrane of pore size 250-500 μm. The physical activation of camel bone samples was carried out by carbonizing at 500°C under N_2 gas for 2 h, followed by sample activation under CO_2 gas for 2 h at 600°C (HAp_a) and 900°C (HAp_b). The elemental chemical analysis of the natural hydroxyapatite was carried out from camel bone [14].

2.3 Preparation of Natural Hydroxyapatite/Cellulose Composite

Cellulose fibre was first dispersed in water for 24 h. Then, 0.5 g of wet cellulose was immersed in 100 mL water containing 0.1 g of HAp_a or HAp_b. After refluxing for 4 h, the samples were washed well with distilled water and dried at 25 °C.

2.4 Physicochemical Characterizations

2.4.1 FTIR Study

The FTIR spectra of the prepared composites were recorded using a Thermo Scientific Nicolet FTIR spectrometer. The samples were carefully grounded, mixed well with the KBr powder, and then pressed in the form of a disk before analysis [17].

2.4.2 X-ray Diffractometry

Diffractograms were recorded at 25 °C with Rigaku Print 2200V series using the Ni-filtered Cu Kα radiation (λ = 1.54 Å). The operating voltage and current were 40 kV and 30 mA respectively[18].

2.4.3 Determination of Crystallinity Index

Crystallinity was calculated from the diffracted intensity data using the method as reported by Segal *et al.*[19]. The crystallinity index (CI) values were obtained using the following equation:

$$CI\% = (I_{002} - I_{am})/I_{002} \times 100 \quad \ldots(1)$$

where I_{200} is the maximum intensity of the diffraction from the (200) plane at 2θ = 22.8°, and I_{am}, the intensity of the amorphous background scatter measured at 2θ = 18°.

2.4.4 Determination of Crystallinity Width

The crystallite widths (CW) of cellulosic fibres were estimated and evaluated using Scherer's equation. The evaluations were performed using the peak profile of the (200) reflection at 2θ = 22.8° that refers to the width of the crystallite[20]. Scherer's equation is given below:

$$L = K\lambda/\beta \cos\theta \quad \ldots(2)$$

where L is the crystallite width; θ, the Bragg angle; λ, the wavelength of the radiation; K, a constant; and β, the corrected width of the peak given by the specimen. A value of K = 0.9 at half-width of the peak profiles was used [20].

2.4.5 Porosity of Natural Hydroxyapatite/Cellulose Composite

The porosity was determined by using the liquid displacement method[19]. The procedure was as follows. At first, the volume (V_0) and weight (W_0) of the sample were measured. Secondly, the sample was immersed in the dehydrated alcohol for 48 h until it was saturated by the absorbing dehydrated alcohol. After that, the sample was weighed again, and the weight was denoted as W_1. Finally, the porosity of the sample was calculated using the formula:

$$P = (W_1 - W_0)/(\rho V_0)$$

where ρ represents the density of the dehydrated alcohol.

2.4.6 Compressive Strength

The compressive strength was tested using a universal material testing machine (AG–10AT, Japan) with a compression strain rate of 5 mm min^{-1} until 50% reduction in the specimen height. The sample was cut into cylindrical blocks with a dimension size 6 × 12 mm. Five parallel samples were tested and the mean value of the compressive strength of different samples was calculated.

2.4.7 SEM Study

The morphology of the samples was examined by using field emission scanning electron microscopy

(FESEM). Images were obtained using an FESEM JEOL 6340 electron microscope.

2.4.8 Thermal Analysis

Thermogravimetric analysis was performed (25–500°C) using a thermogravimetric analyzer (TGA–50, Shimadzu, Japan). The nitrogen flow and heating rates were 20 mL min^{-1} and 20°C min^{-1} respectively, to assess the effect of HAp on the thermal behavior of cellulose.

2.4.9 Kinetics of Thermal Decomposition

The analysis of TGA and DTGA curves was performed by using two different procedures, namely Coats–Redfern (CR) and Horowitz–Metzger (HM) methods [21, 22]. According to the Coats–Redfern method following equation can be obtained for the first-order reaction:

$$\ln\left[\frac{-\ln(1-\alpha)}{T^2}\right] = \ln\left(\frac{AR}{\varphi E}\right) - \frac{E}{RT} \quad \ldots(3)$$

where E is the activation energy; A, the pre-exponential factor; R, the gas constant; α, the fraction of the sample decomposed at time t; φ, the heating rate; and T, the temperature. Plotting $\ln(-\ln(1-\alpha)/T^2)$ versus $1/T$ as per Eq. 3 is found to be linear and gives E^* from the slope and A from the intercept value. For comparative purposes, the activation energy was also determined by the first-order Horowitz–Metzger method according to following equation:

$$\ln\left[-\ln(1-\alpha)\right] = \frac{E}{RT_m}\Theta \quad \ldots(4)$$

where and $\Theta = T - T_m$ and T_m are the peak temperature. A plot of ln[-ln(1-α)] against Θ was found to be linear. E was obtained from the slope and the pre-exponential factor ($A = Z$) was deduced from the following relationship:

$$Z = \frac{E\varphi}{RT_m^2}\exp\left(\frac{E}{RT_m}\right) \quad \ldots(5)$$

Based on the values of activation energy and the pre-exponential factor, the values of the entropy of activation (ΔS^*), the enthalpy of activation (ΔH^*), and the Gibbs free energy (ΔG^*) were calculated by using the following equations:

$$\Delta S^* = R\ln\left(\frac{Ah}{K_B T_m}\right) \quad \ldots(6)$$

$$\Delta H^* = E - RT \quad \ldots(7)$$

$$\Delta G^* = \Delta H^* - T\Delta S^* \quad \ldots(8)$$

where K_B is the Boltzmann constant; h, the Plank's constant; and T_m, the DTGA peak temperature.

3 Results and Discussion

The interaction between the cellulose and natural HAp was studied using the FTIR analysis. Figure 1 shows the FTIR spectra of both cellulose and different activated HAp/cellulose composites. Peaks in the region around 700 cm^{-1} exhibit complex vibrational mode due to skeletal mode vibrations of the pyranose ring in the glucans chain[2]. The hydroxyl group stretching in cellulose is located at 3416 cm^{-1}. The bending modes of the OH vibrations for the primary and secondary hydroxyls [2] are located at 1431–1319 cm^{-1}. The C–O stretching vibration is observed at 1115 cm^{-1}. A decrease in the band size of both the secondary hydroxyl group bending (1431–1319 cm^{-1}) and the C–O stretching vibration (1115 cm^{-1}) confirms the composite formation[3]. The band positioned at around 1650 cm^{-1} corresponds to the bending mode of the naturally absorbed water [22]. On the other hand, the absorption bands at around 660 cm^{-1} and 600 cm^{-1} are attributed to the O–P–O bending vibration in both HAp samples. The bands allocated to PO_4^{3-} groups are observed at 1031 cm^{-1}, 672 cm^{-1}, 560 cm^{-1}, and 520 cm^{-1}. The shoulder peaks at 898 cm^{-1} and 1374 cm^{-1} indicate $HPO_4^{2-}$and CO_3^{2-} incorporation into the amorphous region of

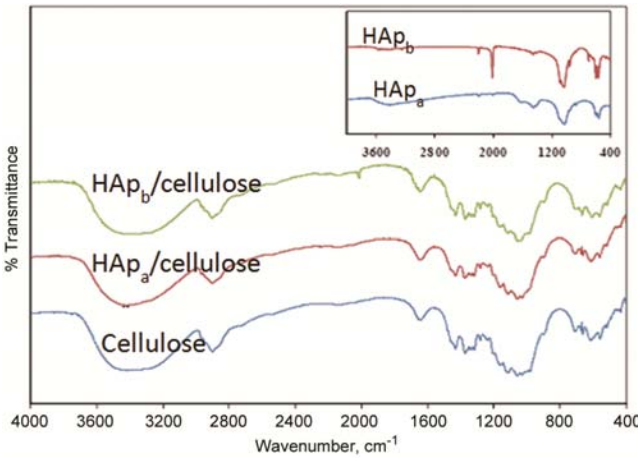

Fig.1 — FTIR spectra of cellulose, HAP_a / cellulose, and HAP_b / cellulose composite (inset: FTIR spectra of HAP_a and HAP_b)

cellulose, where biological HAp contains both $CaCO_3$ and HPO_4 [23-25].

The XRD pattern of cellulose clearly exhibits the typical diffraction peaks at 14.8°, 16.3°, 21.1°, 22.5°, and 34.7° that belong to the (101), (1$\bar{0}$1), (021), (002), and (040) planes of the crystalline structure of cellulose I (Fig. 2 and Table 1)[2]. The characteristic peaks of HAp are represented at 37.4° and 44.06° that could be assigned to the (310) and (222) planes respectively[14]. In Table 1, there are differences between the d-spacing of cellulose and their composites, indicating that the HAp crystals are implanted in cellulose layers. Furthermore, the first peak of HAp at $2\theta = 37.4°$ in the HAp_b /cellulose is disappeared with a low intensity for the second peak at $2\theta = 44.5°$. It may be attributed to the fact that the HAp_b interaction is more than that of HAp_a with cellulose as reflected in the d values of different planes of cellulose (Table 1).

The pore size is determined with a liquid displacement method using dehydrated ethanol as the displacing liquid, where the porosity of the HAp/cellulose composite samples is decreased to 25% in the presence of HAp_a and 38% in the presence of HAp_b. These results indicate that HAp_b is more active towards cellulose than HAp_a. The porosity and compressive strength values for cellulose are found to be 0.00369 & 1; for HAp_a/cellulose, 0.00278 & 1.5; and for HAp_b/cellulose, 0.00227 & 2.2 respectively.

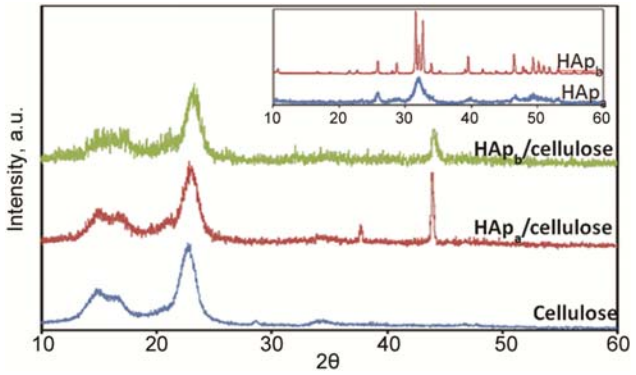

Fig. 2 — X-ray diffractograms of cellulose, HAp_a / cellulose and HAp_b / cellulose composite (inset: XRD's for HAp_a and HAp_b)

Furthermore, the compressive strength measurement also confirms the porosity results. The strength depends chiefly on total porosity and pore size distribution[26]. In general, strength increases as the proportion of larger pores is decreased. It is observed that composite has more compressive strength than cellulose. Moreover, the compressive strength value of HAp_b/ cellulose is the highest as compared to HAp_a/cellulose. From all these results, HAp_b is more reactive than HAp_a towards cellulose. Figure 3 shows the SEM micrographs of the cellulose fibre and the HAp/cellulose composites. As can be seen in the figure, the presence of HAp on the surface is detected, indicating that HAp could penetrate the network structure to form particles throughout the cellulose fabric. Particles are appeared to be well bonded to the cellulose fibres, which is helpful to improve the mechanical properties of the cellulose. Furthermore, the particles in HAp are uniformly dispersed, indicating that the HAp particles are homogeneously distributed in the cellulose matrix, especially in the HAp_b/cellulose. The fibre width in the composites is less than that in cellulose (Fig.3). It may be attributed to the highest compressive strength with less pore size.

Thermogravimetric analysis is an important method for investigating the probability of attachment of solvent molecules or hydrated water, besides the thermal degradation behavior as shown in Fig. 4. Based on the observation of mass loss data, cellulose shows significant mass losses, first at 309–433°C (54.5%) and then at 434-495°C (18.0%). In comparison, both the composites show significant mass losses at higher temperatures [311–490°C (48.8%) and 325–497° (76.2%) respectively].

Table 1 — Degree of crystallizations index (CI) and crystallite size (CS) at (200) plan of cellulose and its composites

Composite	CI	CS	Lattice plane, deg				
			(101)	(1$\bar{0}$1)	(021)	(002)	(040)
Cellulose	881	00.36	14.98	16.34	20.60	22.86	34.23
			(5.91)	(5.42)	(4.31)	(3.88)	(2.61)
HAp_a/cellulose	778	00.55	14.86	16.62	20.76	22.90	34.19
			(5.96)	(5.33)	(4.27)	(3.88)	(2.62)
HAp_b/cellulose	772	00.61	15.38	16.90	21.12	23.13	34.38
			(5.70)	(5.21)	(4.19)	(3.84)	(2.60)

Values in parenthesis are inter-planer distance (d).

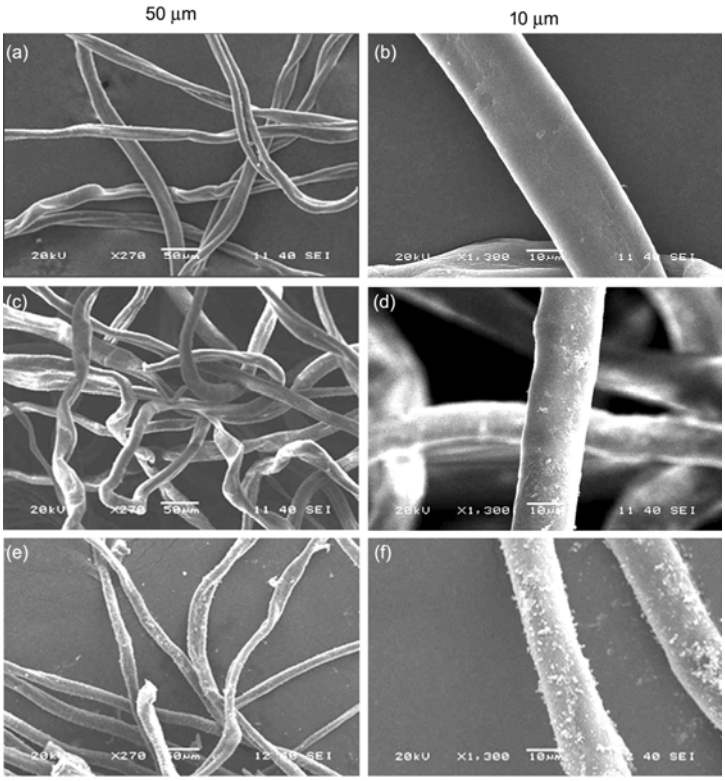

Fig.3 — SEM micrographs of cellulose (a & b); HAp_a / cellulose composite (c & d); and HAp_b / cellulose composite (e & f)

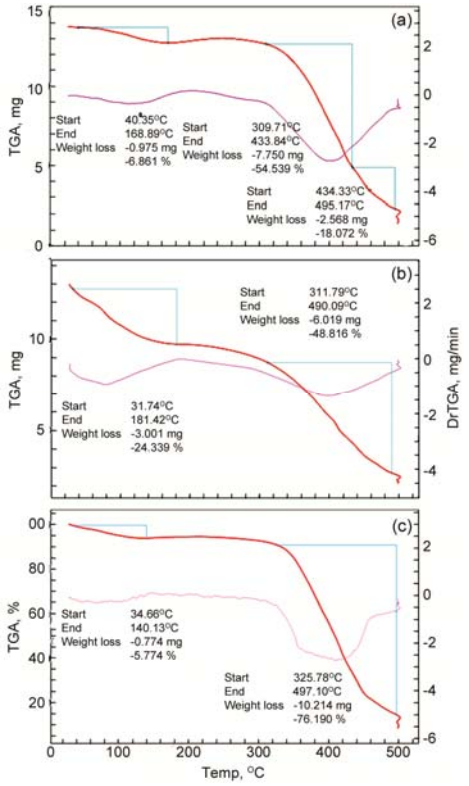

Fig. 4 — TGA and DTGA curves for (a) cellulose (b) HAp_a / cellulose and (c) HAp_b/ cellulose

Table 2 — Thermal decomposition data for cellulose and HAp/cellulose composites

Compound	Step	TG/DTG, °C			Weight
		T_i	Tm	T_f	loss, %
Cellulose	1st	40	195	168	6.86
	2nd	309	320	433	54.54
	3rd	434	465	495	18.07
HAP_a/ cellulose	1st	32	108	181	24.34
	2nd	312	401	490	48.82
HAP_b/ cellulose	1st	35	90	140	5.57
	2nd	326	410	497	76.19

T_i – Initial temperature, T_m – Maximum temperature and T_f – Final temperature.

This increase in decomposition temperature suggests that the thermal stability of composites is higher than that of cellulose. The thermal data and calculated thermodynamic parameters (E, ΔH^*, ΔS^*, and ΔG^* values) are presented in Tables 2 and 3. Two methods, namely CR and HM, are used to calculate the thermal degradation kinetic parameters. As can be seen from Table 3, E is obtained with a correlation coefficient greater than 0.9999. Furthermore, different E and ΔH^* values are obtained for the cellulose and $HAp_{a,b}$/cellulose composites. These different values

Table 3 — Thermodynamics activation parameters for cellulose and HAp /cellulose composites using Coats-Redfern (CR) and Horowitz-Metzger (HM) methods for 2nd step

Compound	E, kJ mol^{-1}		*A*, s^{-1}		ΔS*, J mol^{-1} K^{-1}		ΔH*, kJ mol^{-1}		ΔG*, kJ mol^{-1}		DTG_{max} °C
	CR	HM	CR	HM	CR	HM	CR	HM	CR	HM	
Cellulose	295 (r=0.99993)	284 (r=0.99991)	1.50E+18	9.86E+20	96.5	150	254	278	191	180	320
HAP_a/cellulose	103 (r=0.99993)	120 (r=0.99991)	3.26E+05	1.66E+07	146	113	97.2	114	196	191	401
HAP_b/cellulose	112 (r=0.99993)	134 (r=0.99991)	1.68E+06	3.91E+08	132	87.0	107	128	194	168	410

would suggest different degradation mechanisms and binding mechanisms. The highest *E*, Δ*H**, and *A* values are observed for the cesllulose (295 kJ mol^{-1}, 254 kJ mol^{-1}, and 1.50E+18 s^{-1} respectively). On the other hand, both the composites studied show lower values for *E*, i.e 103 kJ mol^{-1} and 112 kJ mol^{-1} in HAp_a/cellulose and HAp_b/cellulose respectively. These lower *E* values could be attributed to the bonding effects due to the blending of HAp with the cellulose. These values also confirm the amorphous and porous nature of the composites compared to the cellulose as also observed by XRD and porosity measurements. Moreover, positive values of Δ*G** are obtained for the cellulose and its composites which indicate no spontaneous decomposition reaction. However, the positive Δ*S** value is obtained for the cellulose and negative Δ*S** values for both the composites, indicating that the activated composites have more ordered structure than the cellulose and hence show a slower decomposition reaction.

4 Conclusion

In this study, we prepared the natural HAp (at two activated temperatures)/cellulose composites by a simple and effective method without applying any other toxic crosslinking agents. The novel HAp_b (activated at 900°C)/cellulose composite was found to have a good porous structure and a high compressive strength. Furthermore, the composites show mass losses at higher temperatures, confirming higher thermal stability as compared to cellulose, conforming with the obtained thermodynamic results.

Acknowledgement

The authors extend their appreciation to the Deanship of Scientific Research at King Khalid University for funding this work through General Research Project under grant number (G.R.P-167-38).

References

1 Keshk SMAS & Sehemi A, *Am J Polym Sci*, 3 (2013) 46.
2 Keshk SMAS, Yousef E & Omran A, *Indian J Fibre Text Res*, 40 (2015)190.
3 Keshk SMAS, Hamdy M & Bader I, *Am J Polyms Sci*, 5 (2015) 29.
4 Keshk SMAS, Salah H, Hamdy M & Badr I, *Physicochemical Characterization of Mercerized Cellulose-Supported Nickel-Oxide*, paper presented at the 18th International Conference on Applied Chemistry, Zurich, Switzerland, 12–13 January 2016
5 Azzaoui K, Lamhamdi A, Mejdoubi E M, Berrabah M, Hammouti B & Elidrissi A, *Carbohyd Polym*, 111(2014) 41.
6 Murugan R & Ramakrishna S, *Biomaterials*, 25 (2004) 3829.
7 Bigi A, Boanini E, Capuccini C & Gazzano M, *Inorg Chim Acta,* 360 (2007)1009.
8 Adzilaa S, Sopyan I, Singh R & Pusparini E, *Indian J Chem*, 52 (2013) 739.
9 Metikos-Hukovic M, Tkalcec E & Kwokal A, *Piljac J Surf Coat Technol*, 165 (2003) 40.
10 Wang Q, Huang W, Wang D, Darvell BW, Day DE & Rahaman M N, *J Mater Sci*, 17 (2006) 641.
11 Ishikaa M, Oaki Y, Tanaka Y, Kakisawa H, Alvarezd G & Imai H, *J Mater Chem B*, 3 (2015) 58.
12 Choi S & Jeong Y, *Fibre Polym*, 9 (2008) 267.
13 Badran H, Yahia IS, Hamdy M S & Awwad N S, *Rad Phys Chem*, 130 (2017) 85.
14 El-Zahhar A A & Awwad N S, *J Environ Chem Eng*, 4 (2016) 633.
15 Moor R C, Holt K, Awwad N S, Gasser M S, Sanchez C H & Hassan Z, *J Radio Chemia Acta*, 91 (2003) 721.
16 Moore R C, Gasser M, Awwad N S, Holt K C, Salas F M, Hasan M, Hasan M A, Zhao H & Sanchez C A, *J Radioanal Nucl Chem*, 263(2005) 97.
17 Abbott T P, Palmer D M, Gordon SH & Bagby M O, *J Wood Chem Technol*, 81(1988)1.
18 Segal L, Creely J J, Martin A E (Jr) & Conrad C M, *Text Res J*, 29 (1959) 786.
19 Jasiukaityte E, Kunaver M & Poljansek I, *Bio Res*, 7 (2012) 3008.
20 Zhang Y & Zhang M, *J Biomed Mat Res*, 55 (2001) 304.
21 Coats A W & Redfern J P, *Nature*, 201 (1964) 68.
22 Horowitz H W & Metzger G, *Anal Chem*, 35 (1963) 1464.
23 Pastorova I B, Botto R E, Arisz P & Boon J J, *Carbohydrate Res*, 262 (1994) 27.
24 Keshk S M A S & Salah M, *Am J Polym Sci*, 4, 10, 2014.
25 Mindess S, *J Am Ceramics Soc*, 53 (1970) 621